Ge *et al.*
Chinese Journal of Mechanical Engineering (2022) 35:51
https://doi.org/10.1186/s10033-022-00713-4

Chinese Journal of Mechanical Engineering

ORIGINAL ARTICLE

Open Access

Formation Principle and Characteristics of Self-Supercharging Pulsed Water Jet

Zhaolong Ge[1,2], Yuanfei Ling[1,2], Jiren Tang[1,2*], Yiyu Lu[3], Yangkai Zhang[1,2], Lei Wang[1,2] and Qi Yao[1,2]

Abstract

High-pressure pulsed water jet technology has considerable development potential in the field of rock fragmentation. To overcome the shortcomings of existing pulsed jets, a self-supercharging pulsed water jet (SSPWJ) generation method is proposed, which is based on the theory of the pulsed water jet and the principle of hydraulic boosting. The proposed method changes the flow direction of the fluid medium through the valve core to make the piston reciprocate in the cylinder and relies on the effective area difference between the front and rear chambers in the stroke stage of the piston to realize the organic combination of "pulse" and "supercharging" of the jet, thus forming an SSPWJ. On the basis of the formation principle of the SSPWJ, a SSPWJ testing platform was constructed, and tests were performed on the jet pressure acquisition, morphology capture, and granite erosion. Both the jet pressure and the jet morphology exhibited periodic changes, and a higher pulse pressure was obtained at lower inlet pressure. The error of the pressure ratio calculated according to the experimental results was <3% relative to the theoretical design value, confirming the feasibility of the method. The pulse pressure and pulse frequency are controllable; that is, as the inlet flow rate increases in the stroke stage of the piston, the pulse pressure and pulse frequency increase, and the pulse duration decreases. As the inlet flow rate increases in the backward-stroke stage of the piston, the pulse frequency increases, and the pulse pressure and pulse duration remain unchanged. Under the combined action of the water-hammer pressure, high-speed lateral flow, and high-frequency dynamic load of the SSPWJ, local flaky exfoliation was observed when the granite surface was eroded. The results of this study lay the foundation for enriching the theory of pulsed jet generation and expanding its application range.

Keywords: Pulsed water jet, Self-supercharging, Pulse parameters, Jet morphology, Granite breaking

1 Introduction

Water-jet technology for rock-breaking is dust-free, non-polluting, and highly efficient [1, 2]. Because of these advantages, it is widely used in mining, tunnelling, and oil drilling [3–6]. The pulsed water jet acts on the target in the form of a pulse, which can cause the rock to produce tensile, shear, and fatigue damage under a low jet pressure and form macrocracks that lead to volume fracture by effectively applying the water-hammer effect of the jet to the target, the stress wave under the impact, and the pulsed cyclic shock [7–10]. Research results indicate that the erosion ability of the pulsed jet is significantly higher than that of the continuous water jet under the same pressure and that the specific energy consumption is lower [11–13].

The existing pulsed jets are mainly divided into four types: percussion pulsed jets, disc-slotted pulsed jets, ultrasonic modulated pulsed jets, and self-excited oscillation pulsed jets. The percussion pulsed jet is generated by using a flywheel or freefalling heavy hammer as the power source to transfer energy to the compression piston. The water in the cavity is quickly extruded after the compression piston receives the energy, as shown in Figure 1a. Sdehkhoda et al. [14–17] established a dynamic model for the cavity pressure and determined

*Correspondence: jrtang2010@163.com
[1] State Key Laboratory of Coal Mine Disaster Dynamics and Control, Chongqing University, Chongqing 400030, China
Full list of author information is available at the end of the article

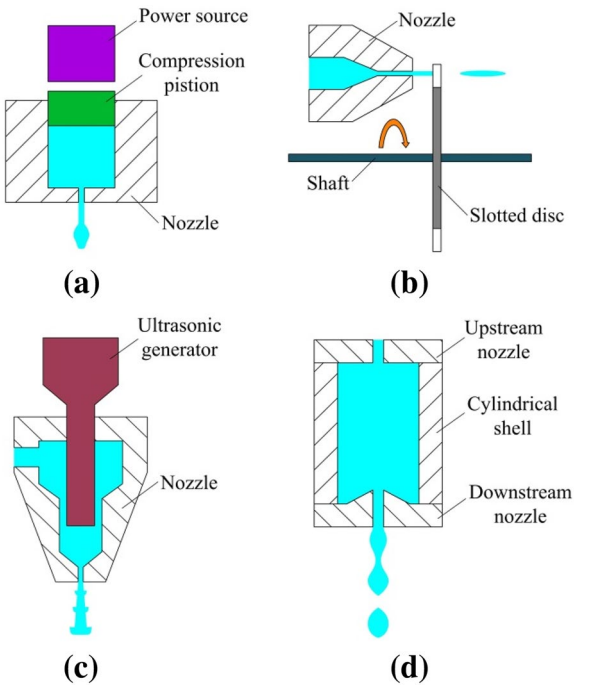

Figure 1 Types of pulsed jets

the relationships between the liquid height of the cavity, piston mass, nozzle diameter, and pulse pressure. This method can form a large-diameter and high-speed pulsed jet; however, the formation process is complex, water injection and resetting are required before each operation, and continuous emission cannot be performed. For the disc-slotted pulsed jet, the continuous jet is periodically cut with a slotted disc, dividing it into a series of discrete jet segments, as shown in Figure 1b. Dehkhoda et al. [18, 19] found through rock breaking experiments that the formation, crack propagation, and internal damage of rock craters are related to the pulse length and pulse frequency. The pulse length and pulse frequency can be controlled by changing the slot width, number of slots, and rotational speed of the disc. Reasonable rock-breaking parameters can be selected according to the research results; however, the jet pressure depends on the pump pressure, and jet deflection will cause energy loss during the jet-cutting process. The ultrasonic modulated pulsed jet concentrates the ultrasonic energy through an ultrasonic generator, and a high-density sound field is applied to the fluid inside the nozzle to cause a periodic change in the pressure before the ejection, as shown in Figure 1c. Refs. [20–22] use this pulsed jet with 20 or 40 kHz pulse frequency to perform cutting experiments on sandstone and bone cement. The nozzle exit velocity field and flow-pattern change were examined. The fluctuation rate of the jet velocity gradually decreased with an increase in the jet distance. For rock-cutting experiments, it is necessary to strictly control the target distance, and it is difficult to eliminate the "water-cushion effect" on the target body due to the high pulse frequency. The basic principle of the self-excited oscillation pulsed jet is that the fluid passes through the resonant chamber, which is commonly referred to as the Helmholtz oscillating chamber, so that the fluid produces steady-stage oscillation of a certain frequency, and the jet pressure exhibits a macroscopic change, as shown in Figure 1d. Refs. [23–27] reveal the effects of the pump pressure and oscillating chamber structure on the pressure fluctuations through experimental research. Although a high-frequency pulsed jet can be formed, the pressure fluctuation amplitude is not significant when the pump pressure is high, and the requirement for the structure of the oscillating chamber is very strict.

The main pulse parameters affecting the rock-breaking efficiency of the pulsed jet include the pulse pressure, pulse frequency, and pulse duration [18, 19, 28–30]. The four aforementioned types of pulsed jets each have advantages; e.g., the percussion pulsed jet has a high pulse pressure, the pulsed pressure and pulse frequency of the disc-slotted pulsed jet can be controlled, and the generation methods of the ultrasonic modulated and self-excited pulse jets are simple. However, they also have disadvantages for rock breaking. The percussion pulsed jet generation method is complex, and its emission frequency is too low. The disc-slotted pulsed jet cannot produce a supercharging effect. The ultrasonic-modulation and self-excited pulsed jets have limited pressure fluctuations, and the frequency adjustment is inconvenient. These factors reduce the rock-breaking efficiency, making it difficult to satisfy the application requirements in the field.

In this paper, a SSPWJ generation method based on the theory of the pulsed water jet and the principle of hydraulic boosting is proposed. A higher pulse pressure can be obtained at a smaller inlet pressure through reasonable structural design and piping connection without an additional power source. Both the pulse pressure and the pulse frequency can be adjusted. The proposed method, which is safe and reliable, can not only satisfy the requirements for efficient rock-breaking but also reduce the cost. To validate the feasibility of this method, a self-supercharging pulsed jet generating system was designed, and a test platform was constructed. Pressure acquisition, morphology capture, and granite erosion tests were performed to determine the change law of the pulse parameters and the jet morphology and to evaluate the rock-breaking ability.

2 Generation Method and Formation Principle of SSPWJ

2.1 Generation Method of SSPWJ

The SSPWJ is generated by using a fluid medium as the power source to drive the piston to reciprocate and squeeze the water in the chamber. The pressure energy of pressurized water is converted into kinetic energy through a nozzle and ejected at a high speed. The piston reciprocates once, and the high-pressure water is ejected once. The jet pressure changes periodically because of the intermittent ejections. The action areas of the large and small ends of the piston are not equal. According to the principle of hydraulic boosting, a higher jet pressure can be obtained at a lower inlet pressure. The jet generation method is shown in Figure 2. The piston movement includes two stages: backward-stroke and stroke. When the reversing valve is in the right position, chamber 4 is connected to the oil inlet, chamber 7 is connected to the oil outlet, and the high-pressure fluid enters chamber 4 to push the piston to the right. Chamber 1 is used to supplement water, and chamber 2 is connected to the atmosphere. When end face A1 of the piston moves to chamber 5, chambers 4 and 5 are connected, and the piston backward-stroke ends. The reversing valve switches to the left position, and chambers 4 and 7 are connected to the oil inlet to form a differential connection. Owing to the difference in the effective action area, the high-pressure oil enters chamber 7 to push the piston to the left. The water in chamber 1 is extruded, and forms a jet. When end face A2 of the piston moves to chamber 5, chambers 5 and 6 are connected, the piston stroke ends, the pressure of chamber 1 drops rapidly, the reversing valve switches to the right position, and the next backward-stroke stage of the piston will soon start.

In the SSPWJ generation method, under the continuous injection of fluid, the state of the reversing valve is switched to change the flow direction of the fluid that pushes the piston reciprocating motion to intermittently extrude the water in chamber 1, and the pressure of chamber 1 exhibits periodic changes. During the piston stroke, the jet pressure is higher than the inlet pressure, which can generate a certain pressure ratio. The theoretical pressure ratio is equal to the ratio of the action area difference of the piston in chambers 7 and 4 to the action area of the piston in chamber 1. Therefore, this method can generate a consecutive high-pressure pulse jet without high-pressure components (high-pressure pump, high-pressure hose, high-pressure valve, etc.) under the continuous injection of low-pressure fluid, which is safe and inexpensive.

2.2 Formation Principle of SSPWJ

The SSPWJ generation system is a valve-controlled piston motion system with fluid as the energy-transfer medium. The establishment of the system dynamic model can theoretically reveal the principle of SSPWJ generation.

2.2.1 Dynamic Analysis of System

The piston is the main moving body of the system; it performs the backward-stroke and stroke under the action of oil pressure. The motion equations corresponding to the different motion stages of the piston differ, as shown in Figure 3. To facilitate the derivation and calculation, the following assumptions are made when establishing the equation of motion of the piston: 1) The fluid is not compressible. 2) The temperature, viscosity, and bulk modulus of the fluid are constant. 3) The pistons and other components are absolutely rigid. 4) The mechanical friction loss and oil pressure loss are ignored. 5) Grooves

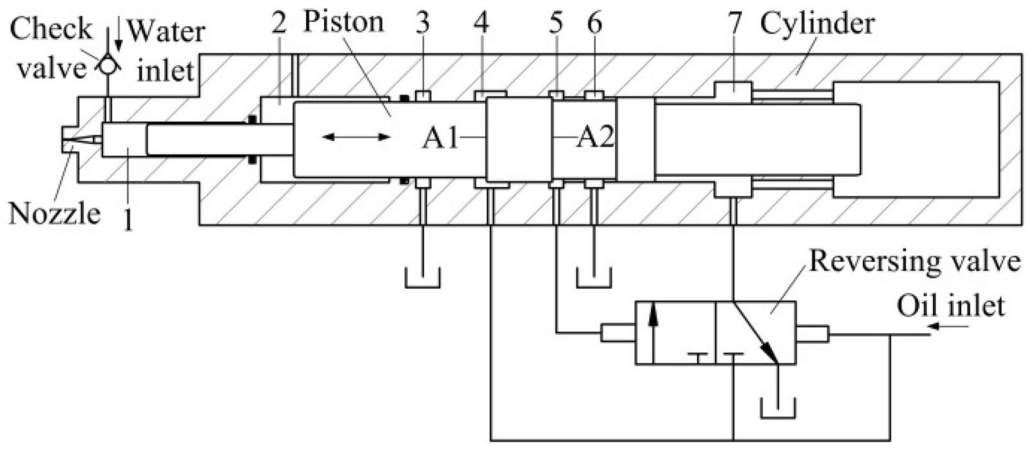

Figure 2 SSPWJ generation diagram

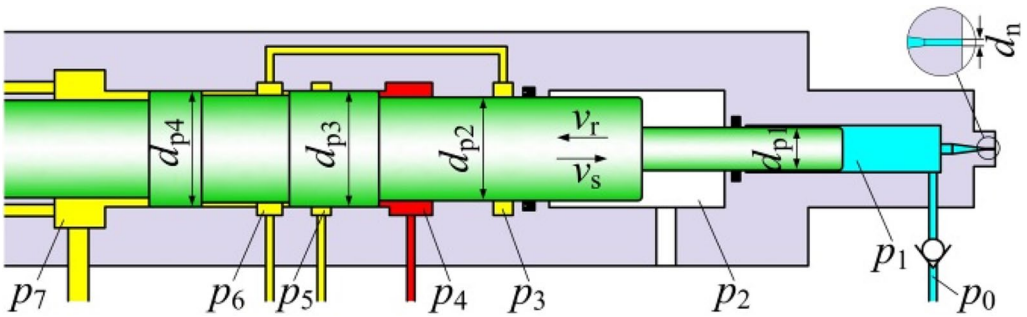

Figure 3 Piston motion diagram

are circumferentially applied to the piston surfaces; thus, the influence of the hydraulic lock force is ignored [31].

When the piston backward-strokes, the dynamic equation is expressed as

$$ma_r = \frac{\pi}{4}[d_{p1}^2 p_1 + (d_{p2}^2 - d_{p1}^2)p_2 + (d_{p3}^2 - d_{p2}^2)p_4 - d_{p4}^2 p_7], \tag{1}$$

where $p_4 = p_{in}$, $p_7 = p_6 = p_3 = p_{out}$, $p_1 = p_0$; m is the mass of the piston, a_s is the backward-stroke acceleration of the piston, p_{in} is the inlet pressure, p_{out} is the outlet pressure, and p_0 and p_2 are the tap water pressure and atmospheric pressure, respectively, which can be ignored.

When the piston strokes, the dynamic equation is expressed as

$$ma_s = \frac{\pi}{4}[d_{p4}^2 p_7 - (d_{p3}^2 - d_{p2}^2)p_4 - (d_{p2}^2 - d_{p1}^2)p_2 - d_{p1}^2 p_1], \tag{2}$$

where $p_4 = p_7 = p_{in}$, $p_6 = p_3 = p_{out}$; a_s is the stroke acceleration of the piston.

2.3 Analysis of Pulse Parameters

The pulse pressure, pulse frequency, and pulse duration are pulse parameters which significantly affect the rock-breaking ability of the pulsed jet. The expressions for the pulse parameters of the SSPWJ can be derived from the pulsed water jet theory and the dynamics equation of the piston.

During the piston backward-stroke, the inlet pressure, outlet pressure, inlet flow rate, and outlet flow rate are expressed as follows:

$$\begin{cases} p_{in} = \dfrac{d_{p_4}^2 p_{out} + \frac{4}{\pi} m a_r}{d_{p_3}^2 - d_{p_2}^2}, \\ p_{out} = k_x q_{out}^2 + k_y \dfrac{q_{out}^2}{A_y^2}, \\ q_{rin} = \dfrac{\pi}{4}(d_{p3}^2 - d_{p2}^2)v_r, \\ q_{out} = \dfrac{\pi}{4} d_{p4}^2 v_r, \end{cases} \tag{3}$$

where q_{out} is the outlet flow rate, k_x is the coefficient related to the pipeline resistance and fluid properties, k_y is the coefficient related to the resistance caused by the throttle valve and fluid properties, A_y is the overflow area of the throttle valve, q_{rin} is the inlet flow rate in the backward-stroke stage of the piston, and v_r is the backward-stroke velocity of the piston.

According to the Bernoulli equation, the relationship between the chamber 1 pressure and the jet velocity can be obtained as follows:

$$v_{jet} = \mu \sqrt{\frac{2p_1}{\rho}}, \tag{4}$$

where v_{jet} represents the jet velocity, μ is the flow coefficient, and ρ is the fluid density.

The flow rate of the nozzle q_n is given as

$$q_n = \frac{\pi}{4} d_n^2 v_{jet}. \tag{5}$$

During the piston stroke, the inlet pressure, outlet pressure, inlet flow rate, and outlet flow rate are expressed as follows:

$$\begin{cases} p_{\text{in}} = \dfrac{d_{p_1}^2 p_1 + \frac{4}{\pi} m a_{\text{s}}}{d_{p_2}^2}, \\ p_1 = \dfrac{8\rho q_{\text{n}}^2}{\pi \mu^2 d_{\text{n}}^4}, \\ q_{\text{sin}} = \dfrac{\pi}{4} d_{p_2}^2 v_{\text{s}}, \\ q_{\text{n}} = \dfrac{\pi}{4} d_{p_1}^2 v_{\text{s}}, \end{cases} \tag{6}$$

where q_{sin} is the inlet flow rate in the stroke stage of the piston, and v_{s} is the stroke velocity of the piston.

According to Eq. (6), the chamber 1 pressure can be expressed as

$$p_1 = \frac{8\rho d_{\text{p}_1}^4 q_{\text{sin}}^2}{\pi^2 \mu^2 d_{\text{n}}^4 d_{\text{p}_2}^4}. \tag{7}$$

The chamber 1 pressure is converted into the jet dynamic pressure, which is expressed as

$$p_{\text{jet}} = \frac{1}{2}\rho v_{\text{jet}}^2 = \mu^2 p_1. \tag{8}$$

The theoretical pressure ratio i is given as

$$i = \frac{d_{\text{p2}}^2}{d_{\text{p1}}^2}. \tag{9}$$

The travel distance of the piston h is given as

$$h = \int_0^{t_{\text{r}}} v_{\text{r}} \mathrm{d}t = \int_0^{t_{\text{s}}} v_{\text{s}} \mathrm{d}t, \tag{10}$$

where t_{r} is the backward-stroke duration of the piston, and t_{s} is the stroke duration of the piston, which is also the pulse duration.

According to Eqs. (3), (6), and (10), the travel distance of the piston can be expressed as

$$h = \int_0^{t_{\text{r}}} \frac{4q_{\text{rin}}}{\pi(d_{\text{p3}}^2 - d_{\text{p2}}^2)} \mathrm{d}t = \int_0^{t_{\text{s}}} \frac{4q_{\text{sin}}}{\pi d_{\text{p2}}^2} \mathrm{d}t. \tag{11}$$

The pulse frequency (f, in Hz) is expressed as

$$f = \frac{1}{t_{\text{r}} + t_{\text{s}}}. \tag{12}$$

From Eqs (7), (8), (11), and (12), the jet pressure p_{jet} depends on the working parameter q_{sin} and the structural parameters d_{p1}, d_{p2}, and d_{n}; the pulse frequency f depends on the working parameters q_{rin} and q_{sin} and the structural parameters h, d_{p2}, and d_{p3}; and the pulse duration t_{s} depends on the operating parameter q_{sin} and the structural parameters h, d_{p1}, d_{p2}, and d_{n}.

3 SSPWJ Generation System Design

3.1 Generation Device Design

The self-supercharging pulsed jet generation device is the power mechanism of the system, which is mainly composed of the piston, valve core, and cylinder, as shown in Figure 4. The piston is used to pressurize the low-pressure water in chamber 1, the valve core is used to reverse the movement of the piston, and the continuous generation of the pulsed jet is realized via the motion coupling of the piston and valve core. It is necessary to reasonably design the structure of the piston and the valve core and the connection of inner chamber of the device.

Both the piston and the valve core are stepped shafts. The diameter of the moving part between them and the cylinder satisfies the relationship $d_{\text{v3}} > d_{\text{v4}} > d_{\text{v2}} = d_{\text{v1}}$, $d_{\text{v3}} > d_{\text{v4}} > d_{\text{v2}} = d_{\text{v1}}$. The side wall of the valve core is provided with a throttle groove and a throttle hole. Five oil chambers are formed between the piston and the cylinder, which correspond to chambers 3–7, respectively, and five oil chambers are formed between the valve core and the cylinder, which correspond to chambers 3–7, respectively. The chambers are connected by internal channels. Chambers 4 and 8 are connected to the P port, and chambers 3, 6, 10, and 12 are connected to the T port. Chambers 7 and 9 are connected, and chambers 5 and 11 are connected.

3.2 Generation System Design

On the basis of the generation device, a self-supercharging pulsed jet generation system was designed, as shown in Figure 5. In addition to the generation device, the system includes a power source, a pressure-acquisition system, and an image-collection system.

The power source mainly consists of an oil pump, a relief valve, and a throttle valve. The oil pump provides power for the generation of the self-supercharging pulsed jet, the relief valve regulates the inlet pressure, and the throttle valve adjusts the pulse frequency. The frequency-regulation principle of the throttle valve is

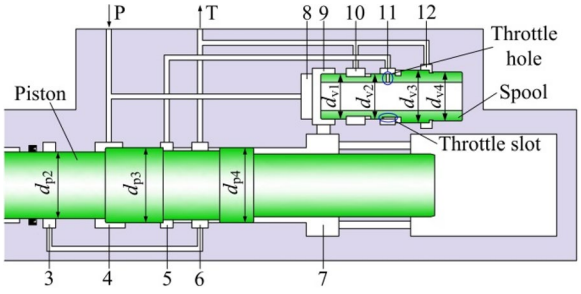

Figure 4 Structure of the SSPWJ generation device

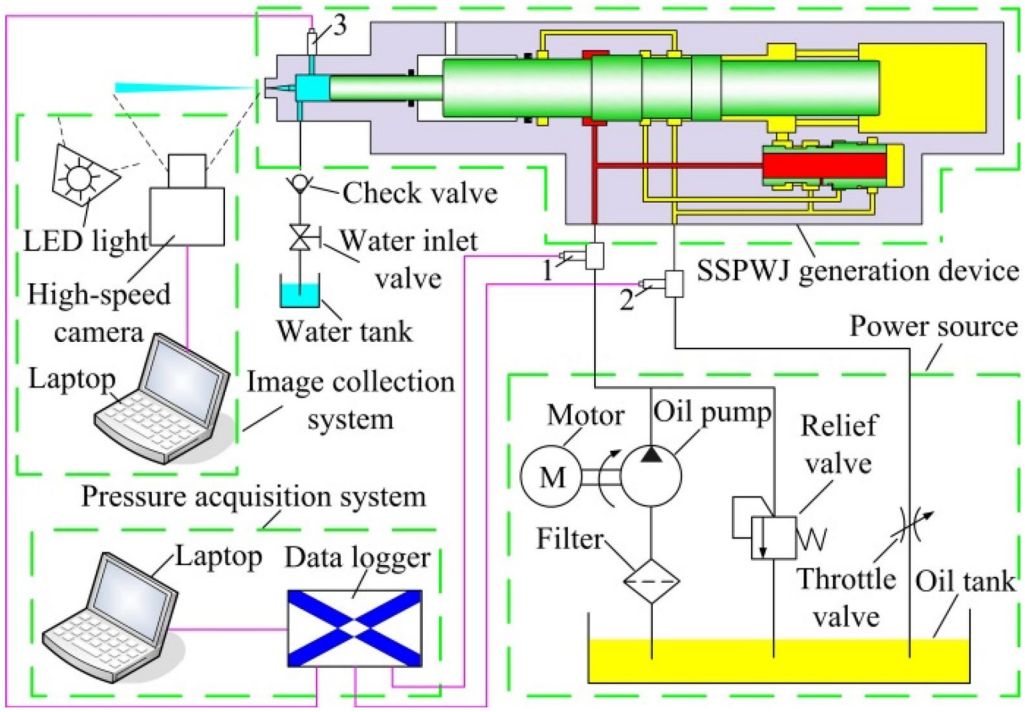

Figure 5 Schematic of the SSPWJ pressure test system

as follows: The structural parameters of the device are fixed. According to Eqs. (3), (11), and (12), if the inlet flow area A_y is reduced without changing the inlet pressure, the outlet flow rate q_{out} decreases, the backward-stroke velocity v_r of the piston decreases, and the backward-stroke time t_r increases, but the stroke time t_s is constant, the pulse frequency f will decrease and vice versa. A throttle valve is added to the oil-return pipeline to adjust the pulse frequency without changing the pulse pressure.

The pressure-acquisition system consists of a pressure sensor, data collector, and laptop. Three pressure sensors are used to measure the inlet pressure, pulse pressure, and outlet pressure. The pressure sensor is connected to the data collector, and the pressure can be monitored and recorded in real time through the acquisition software on the laptop.

The image-collection system consists of a high-speed camera, a light-emitting diode, and a laptop. The generation of self-supercharging pulsed jets is visualized by capturing the change of jet morphology.

3.3 Working Process of System

The formation process of the SSPWJ corresponds to the six movement stages of the piston, as shown in Figure 6. Among them, the yellow area represents low-pressure oil, the red area represents high-pressure oil, the light blue area represents low-pressure water, and the dark blue area represents high-pressure water.

Stage one involves the backward-stroke accelerated movement of the piston, as shown in Figure 6a. The high-pressure oil is divided into two parts. The first part enters chamber 8, because the upper-end surface area of the valve core is larger than the lower-end surface area, the valve core is pushed to the bottom dead-center by the high-pressure oil, and chambers 9 and 10 are connected at this time. The second part enters chamber 4 and drives the piston backward-stroke acceleration. The low-pressure oil in chamber 7 passes through chambers 9 and 10 and then reaches the oil outlet. As the volume of chamber 1 increases, the low-pressure water passes through the check valve; thus, water is supplied to chamber 1.

Stage two involves the backward-stroke uniform movement of the piston, as shown in Figure 6b. Because the outlet pressure increases with the outlet flow rate, the piston will be balanced beyond a certain displacement and enters a uniform-movement stage. Chambers 5 and 6 are disconnected. Chambers 10 and 11 are connected through the throttle slot of the valve core. The oil leaking from chamber 4 to chamber 5 passes through chamber 11, the throttle slot of the valve core, and chamber 10 in turn, finally reaching the oil outlet to ensure that chamber 11 is in the low-pressure stage and the valve core is

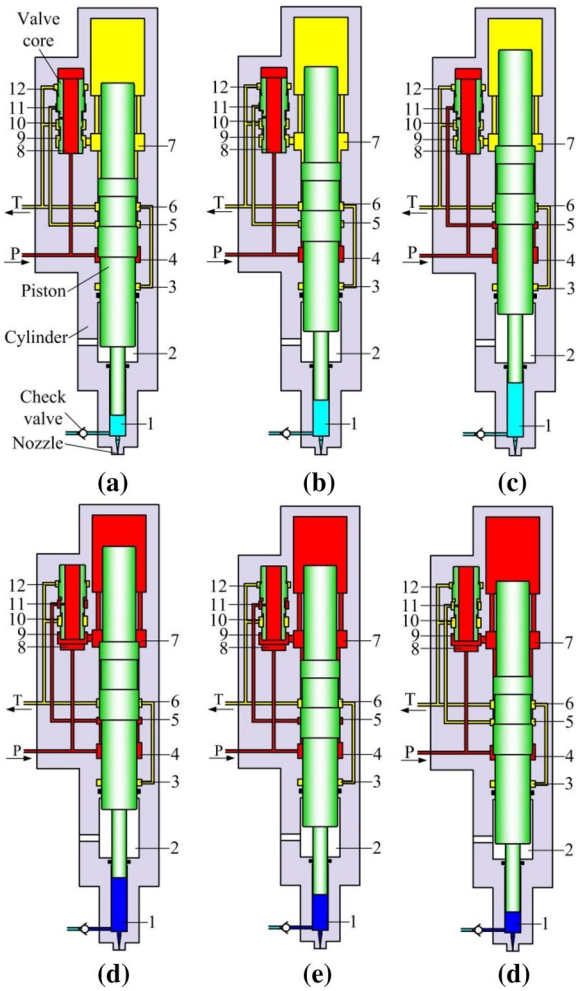

Figure 6 Working process of the system

located at the top dead-center before the end of the backward-stroke movement of the piston.

Stage three involves the backward-stroke deceleration movement of the piston, as shown in Figure 6c. When the front-end surface of the piston moves to chamber 5, chambers 4 and 5 are connected. The high-pressure oil enters chamber 11 through chamber 5. Chambers 8 and 11 are filled with the isobaric high-pressure oil, because the sum of the action area of the bottom-end surface and the action area of the valve core in chamber 11 is larger than the top-end face. The high-pressure oil pushes the valve core to the top dead-center. Chamber 7 changes from a low-pressure chamber to a high-pressure chamber, and the backward-stroke velocity of the piston is reduced to zero.

Stage four involves the stroke decelerated movement of the piston, as shown in Figure 6d. The valve core is located at the top, chamber 8 is connected to chamber 7, the high-pressure oil enters chamber 7 through chamber 8, chambers 4 and 7 are filled with the isobaric high-pressure oil, the action area of the piston in chamber 7 is larger than that in chamber 4, and the high-pressure oil pushes the piston down, while the chamber 1 pressure is rapidly increased, the check valve is closed, and a jet pulse is formed at the nozzle outlet. The high-pressure oil in chamber 3 enters chamber 6 through chamber 7 to form a differential connection.

Stage five involves the stroke uniform movement of the piston, as shown in Figure 6e. Because the pressure of chamber 1 increases with the stroke speed of the piston, the piston will be balanced beyond a certain displacement and enters a uniform-movement stage. The difference in the action area of the piston in chambers 7 and 4 is larger than that in chamber 1. According to the hydraulic supercharging principle, the pressure of chamber 1 is higher than the inlet pressure, and the formed jet has a supercharging effect. After the piston moves a certain distance, chambers 4 and 5 are disconnected, and chambers 11 and 8 are connected through the throttle orifice of valve core to ensure that the 11 chambers are in a high-pressure stage and the valve core is located at the bottom dead-center before the end of the stroke movement of the piston.

Stage six involves the stroke decelerated movement of the piston, as shown in Figure 6f. When the front-end surface of the piston moves to chamber 4, chambers 5 and 6 are connected, and chamber 11 becomes the low-pressure chamber because the top-end surface area of the valve core is larger than the bottom-end surface area. High-pressure oil pushes the valve core to the bottom dead-center. Chamber 7 changes from a high-pressure chamber to a low-pressure chamber, and the stroke velocity of the piston is reduced to zero; thus, a working cycle is completed. Subsequently, the high-pressure oil drives the piston backward stroke and enters the next working cycle.

4 Experimental Research on SSPWJ

4.1 Construction of Experimental Platform

According to the designed experimental system, a performance test platform of the SSPWJ generation device was constructed on the basis of a four-dimensional water jet test experimental platform independently developed by our team. The test was divided into two parts: the first part is the jet pressure-acquisition and morphology-capture test, as shown in Figure 7; the second part is the granite erosion test using the SSPWJ, as shown in Figure 8.

The power source was a hydraulic pump station (model ZYG01B). It was mainly composed of an explosion-proof motor, a duplex gear pump (A pump and B pump), an

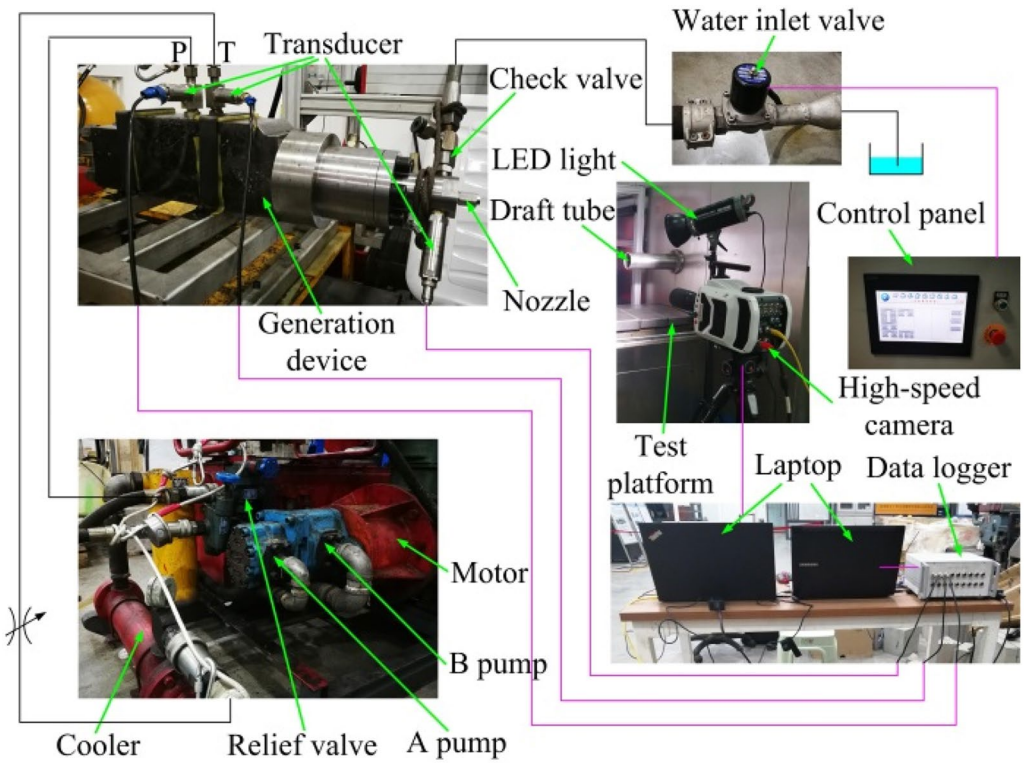

Figure 7 Jet-pressure and morphology test of the SSPWJ

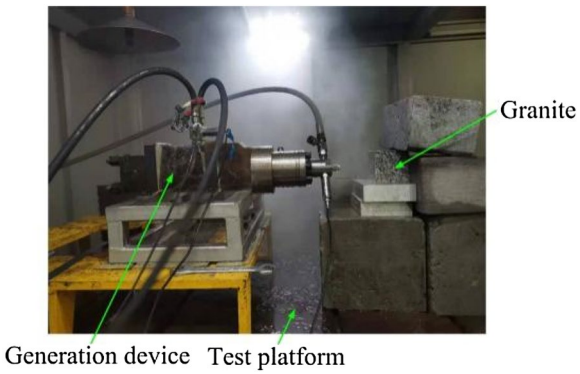

Figure 8 Granite erosion by the SSPWJ

oil tank, a filter, a cooler, and a relief valve. The B pump was used in the experiment, with a rated pressure of 25 MPa and a rated flow rate of 60 L/min. The pressure-regulating range of the relief valve was 0–31.5 MPa. The inlet valve was a solenoid valve controlled by a programmable logic controller. Digital pressure sensors (model XBS100) with a maximum sampling frequency of 100 Hz and an accuracy of 0.1% were used in the pressure-acquisition system. Sensors with ranges of 0–40, 0–20, and 0–120 MPa were connected to the P port, the T port, and chamber 1, respectively. The support frame was fixed on the test platform, the generation device was fixed on the support frame using a U-shaped iron after assembly, and rubber padding was installed for shock absorption. A gem-embedded nozzle with good processing quality was used, which had a flow coefficient of approximately 1. It can be considered that the experimentally measured chamber 1 pressure was equal to the jet dynamic pressure. The image-acquisition system employed a Phantom v2012 high-speed camera.

According to the experimental requirements, the main structural parameters of the device were designed, as shown in Table 1. To evaluate the erosion performance of the SSPWJ, standard 100 mm×100 mm×100 mm cubic granite samples without obvious joints and cracks were selected for the jet erosion test. The main mechanical parameters are presented in Table 2.

4.2 Construction of Experimental Platform

Table 3 presents the parameters of the jet pressure-acquisition and morphology-capture tests. In the first five sets of experiments, the maximum opening of the throttle valve was kept constant, corresponding to an opening value of 1. Only the inlet pressure was changed; the inlet

Table 1 Structural parameters of SSPWJ generation device

d_{p1} (mm)	d_{p2} (mm)	d_{p3} (mm)	d_{p4} (mm)	d_n (mm)	h (mm)	i
22	53	60	60	0.45	35	5.8

Table 2 Mechanical parameters of granite

Bulk density (kg/m^3)	Elastic modulus (mm)	Poisson ratio	Compressive strength (mm)	Tensile strength (mm)
2683	49	0.27	218.2	9.5

Table 3 Parameters of the jet pressure-acquisition and morphology-capture tests

Experiment No.	p_{in} (MPa)	q_{rin} (L/min)	q_{sin} (L/min)	Throttle opening
1	2	2.4	8.5	1
2	4	3.3	11.9	1
3	6	6.2	14.6	1
4	8	8.7	16.8	1
5	10	9.3	18.7	1
6	8	5	16.8	k_1
7	8	2.7	16.8	k_2
8	8	1.6	16.8	k_3
9	8	1.1	16.8	k_4

pressures were set as 2, 4, 6, 8, and 10 MPa. In the last four sets of experiments, the inlet pressure was maintained at 8 MPa, and only the inlet flow rate in the backward-stroke stage of the piston was changed; the throttle valve was set to four different openings. There was no suitable flow meter and pressure sensor for synchronous acquisition, the inlet flow rate in the backward-stroke and stroke stages of the piston could only be determined using the experimental results and the relationship derived in Section 1.2.2. The opening of the throttle valve satisfied the following relationship: $0 < k_4 < k_3 < k_2 < k_1 < 1$.

4.3 Experimental Procedure

Pressure-acquisition and morphology-capture tests were performed outside the platform, using the following procedure. The pipeline and transmission line of the system were connected, and the water inlet valve was opened. The water entered chamber 1 under the action of gravity and generated a low-pressure jet. The high-speed camera lens was aligned with the jet axis and the midpoint of the shooting area, and the shooting frame rate was set as 24722 f/s; that is, the time interval between two consecutive photographs was 40.5 μs. After focusing, a steel ruler was used to calibrate the shooting area. The jet length of each image was 180 mm. The relief valve opening was adjusted to the maximum value, the hydraulic pump was turned on, and the data collection commenced. At this time, the inlet pressure was the minimum, the opening of the relief valve was slowly adjusted according to the inlet pressure displayed on the laptop until the inlet pressure reached the set value, the relief valve was locked, and then the opening of the throttle valve was adjusted. The oil inlet pressure, jet pressure, and oil outlet pressure were collected while capturing the change in the jet morphology at the nozzle exit. After the acquisition was complete, the oil pump and inlet valve were closed, and the data were saved.

Pressure-acquisition and morphology-capture tests were performed outside the platform, and the parameters of group 5 in Table 3 was used as the rock-breaking parameters of the device. To eliminate the influence of the start-up process of the equipment, a steel baffle was placed between the nozzle and the rock sample, and the baffle was quickly removed after the jet stabilized to the required pressure. The erosion time was 2 min, and the target distance was 100 mm. To reduce the error, the erosion test was repeated five times. After the tests, the rock sample was dried naturally in air, and the volume of the erosion pit was measured via the sand-filling method.

5 Results and Discussion

5.1 Analysis of Jet Pressure and Jet Morphology

Figure 9a and b show a part of the experimental results under maximum throttle opening and different oil inlet pressures. The inlet pressure, jet pressure, and return pressure exhibit periodic changes. The supercharging of the jet was generated during the stroke phase of the piston, and the rise, stability, and fall of the jet pressure corresponded to the three stages of stroke acceleration, uniform speed, and deceleration, respectively. The pulse pressure increased with the inlet pressure. Owing to the effects of the diameter and length of the oil-return pipeline, a certain outlet pressure occurred in the backward-stroke phase of the piston, and in the stroke phase of the piston, the outlet pressure was almost zero, which is consistent with the theoretical analysis.

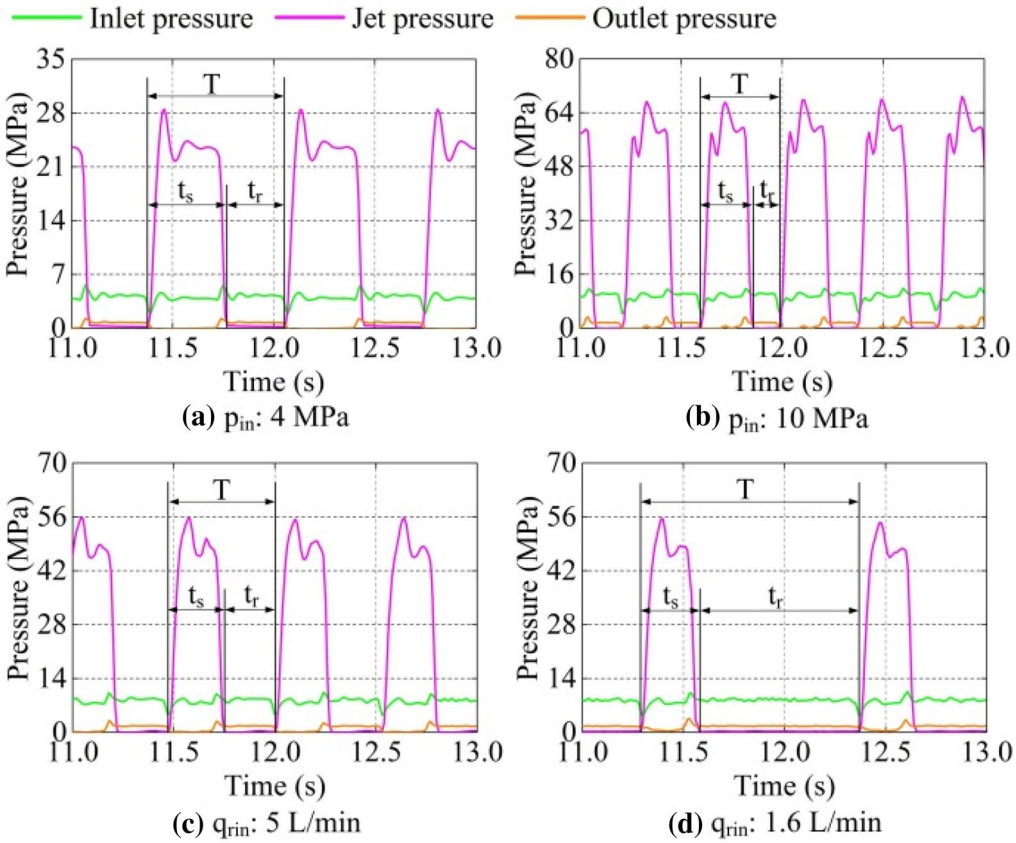

Figure 9 Curves of the inlet pressure, jet pressure, and outlet pressure versus time

Figure 9c and d show a part of the experimental results under constant oil inlet pressure and different throttle openings. The inlet pressure, pulse pressure, and outlet pressure exhibited periodic changes, and the trends were consistent. With an increase in the inlet flow rate in the backward-stroke stage of the piston, the pulse pressure remained unchanged, and the interval between pulses became longer; that is, the backward-stroke time of the piston increased. The frequency-modulation method using meter-out can be used to adjust the pulse frequency without changing the pulse pressure.

As shown in Figure 9, the inlet pressure fluctuated over time, particularly in the rising and falling stages of the pulse pressure, which corresponded to the beginning and end of the piston stroke, respectively. Movement reversal of the piston changed the system load, and the opening of the relief valve produced rapid dynamic changes, resulting in large fluctuations in the flow rate and pressure. It took a period of time for the opening of the relief valve to transition from the dynamic stage to the steady stage; the corresponding inlet pressure had to be stable for a while. In the initial stage of the piston stroke, the jet pressure fluctuated with changes in the inlet pressure owing to the constant pressure ratio. As the inlet pressure increased, the jet-pressure stabilization time decreased, and the fluctuation amplitude increased.

The jet morphology of changed with changes in the jet pressure. The law of the change of the jet morphology was hardly affected by the parameters. The morphology of a single pulsed jet at an inlet pressure of 10 MPa was analyzed, as shown in Figure 10. Frame "a" corresponds to the backward-stroke stage of the piston, where the jet was continuous. The jet pressure was determined by the water inlet pressure. Because of the low water inlet pressure, the nozzle diameter was small, and the jet was thin. Frame "b" corresponds to the initial stage of the piston stroke. When the piston started its stroke, it immediately squeezed the water to form a high-speed jet, which formed an umbrella structure under the action of air friction resistance. As the piston continued to squeeze, the morphology of the jet changed from a thin line to a horn, as shown in frame "c." The increase in the jet velocity increased the amount of entrained air, and the jet boundary gradually expanded to the surroundings. Frame "d" corresponds to the stage of uniform stroke of the piston. During this period, the pulsed jet maintained a horn

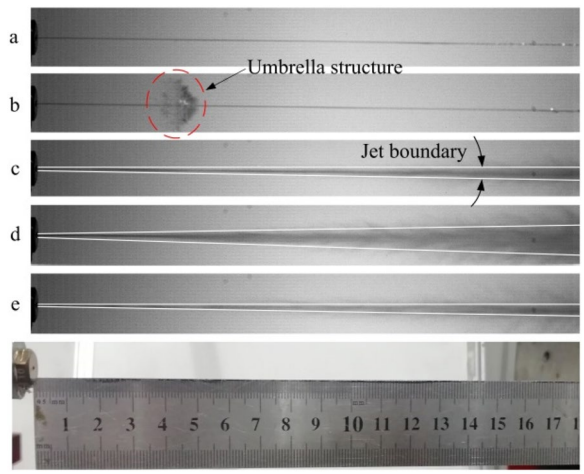

Figure 10 Photographs of the jet morphologies at different times for a single pulse

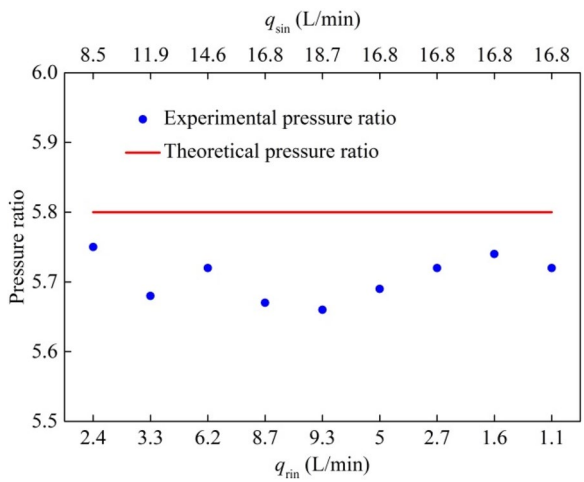

Figure 11 Comparison of the experimental and theoretical pressure ratios under different working parameters

shape, and the jet morphology was stable. Frame "e" corresponds to the stroke deceleration stage of the piston. At this stage, the pulse pressure gradually decreased, the diffusion degree of the jet decreased, and the jet morphology became a thin line again.

5.2 Analysis of Supercharging Effect

The supercharging effect can be reflected by the supercharging ratio, which is the average value of the ratio of the pulse pressure to the inlet pressure, as shown in Figure 11. The supercharging ratio under different working parameters was between 5.67 and 5.75, which is close to the theoretical design value of 5.8, but is lower than the theoretical design value. There are two reasons for this result. On the one hand, the pressure measured in the experiment was the inlet pressure. During the supercharging process, high-pressure oil from the inlet to chamber 7 caused a pressure loss, and the actual pressure of chamber 7 was lower than the inlet pressure. On the other hand, the movement of the piston was affected by the frictional resistance of the seal. In fact, the theoretical design ignores the pressure loss and frictional resistance.

The experimental results confirm the feasibility of the SSPWJ method. Considering the pressure-bearing capacity of the device, the maximum inlet pressure was set as 10 MPa in the experiment. The pulse pressure was determined by the inlet pressure and pressure ratio. By increasing the pressure-bearing capacity of the device or the design value of the pressure ratio under the condition that the flow rate of oil pump is sufficient, a higher pulse pressure can be obtained. Increasing the inlet pressure increases the pressure-bearing capacity of the device, but the inlet pressure is limited by the rated pressure of the pump. If the pressure ratio is increased, a higher inlet flow rate is needed to achieve the desired pulse pressure, but the inlet flow rate is limited by the rated flow rate of the pump. Therefore, both the rated pressure and the rated flow of the pump must be considered in the design of the rated pressure and pressure ratio of the generation device.

5.3 Analysis of Pulse Frequency and Pulse Duration

According to the experimental results and the equations presented in Section 1.2.2, the relationship between the inlet flow rate and the pulse frequency or pulse duration when the opening of throttle valve was maximized was calculated, as shown in Figure 12(a). When the inlet flow rates in the backward-stroke and stroke stages of the piston were increased from 2.4 to 9.3 L/min and from 14.8 to 33 L/min, respectively, the pulse frequency increased from 0.9 to 2.56 Hz, and the pulse duration decreased from 0.54 to 0.25 s. Increasing the inlet flow rate in the backward-stroke phase of the piston will increase the backward-stroke velocity of the piston. Similarly, increasing the inlet flow rate in the stroke phase of the piston will increase the stroke speed of the piston. The travel distance of piston is determined by the structure of the device and remains unchanged, so that the reciprocation period of piston is shortened and the pulse frequency is increased. The pulse duration corresponds to the stroke duration of the piston, the acceleration of the stroke velocity of piston makes the pulse duration shorter.

When the inlet pressure is 8 MPa, the relationship between the inlet flow rate and the pulse frequency or pulse duration is shown in Figure 12(b). The inlet flow rate in the stroke stage of the piston remained unchanged

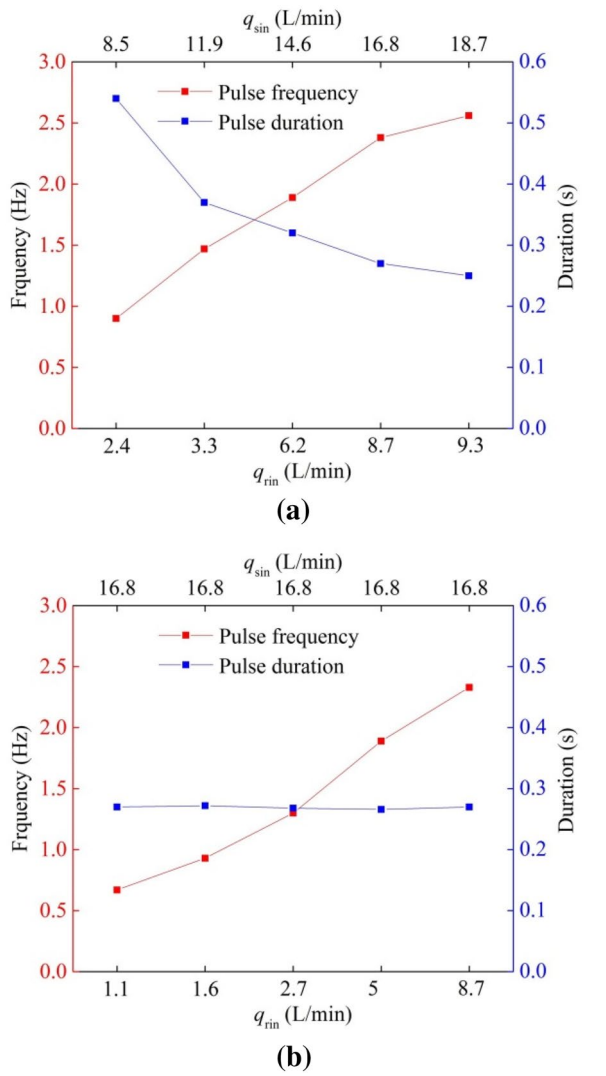

Figure 12 Pulse frequency and pulse duration versus inlet flow rate curve

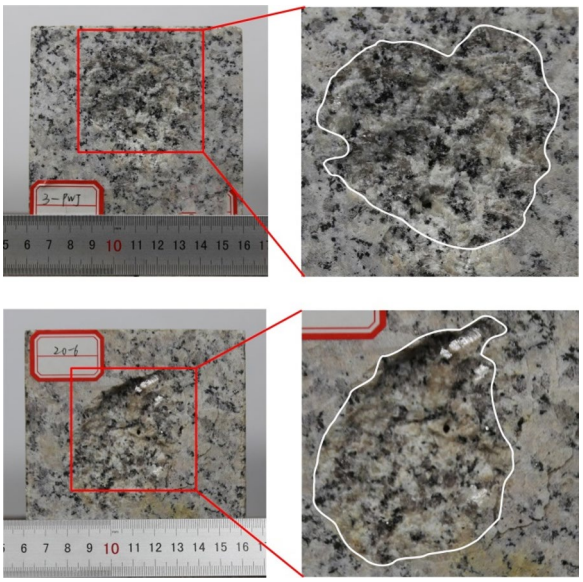

Figure 13 Erosion of granite samples by the SSPWJ

at 29.7 L/min, when the inlet flow rate in the backward-stroke phase of the piston increased from 1.1 to 8.7 L/min, the pulse frequency increased from 0.67 to 2.33 Hz, and the pulse duration was maintained at approximately 0.27 s. The pulse frequency depended on the stroke velocity and backward-stroke velocity of the piston, whereas the pulse duration depended only on the stroke velocity of the piston. The inlet flow rate in the stroke phase of the piston remained unchanged; thus, the stroke velocity of the piston did not change. As the inlet flow rate in the backward-stroke stage of the piston increased, the backward-stroke velocity increased. The travel distance of the piston remained unchanged; thus, the reciprocation period of the piston was shortened, the pulse frequency increased, and the pulse duration remained constant. Owing to the effects of the diameter and length of the oil-return pipeline, oil-return resistance was always generated. If the diameter of the oil-return pipeline is increased and the length is reduced, the oil-return resistance can be reduced, and the return velocity of the piston can be increased. The pulse frequency can be further increased under a constant inlet pressure.

The pulse pressure, pulse frequency, and pulse duration of the SSPWJ were adjusted, providing guidance for the parameter selection of subsequent rock-breaking experiments. The inlet flow rate in the stroke stage of the piston determined the pulse frequency and pulse duration, whereas the change in the inlet flow rate in the backward-stroke stage of the piston only played the role of frequency modulation. Additionally, other structural parameters of the device, such as the piston diameter, nozzle diameter, and travel distance of the piston, affected the pulse frequency and pulse duration. The influence law needs to be studied further, which will provide a basis for the optimal design of the generation device structure.

5.4 Analysis of Granite Erosion by SSPWJ

Under the action of fixed-point erosion by the SSPWJ, flake peeling occurred in a large area of the granite surface, as shown in Figure 13. The rock-breaking process was as follows. First, the jet high-frequency impact caused fatigue damage to the rock surface, and shear failure and tensile failure occur. The broken rock debris was washed away by water, forming an initial erosion

pit. Second, the stress waves generated by the impact dynamic load interfere with each other, resulting in microcracks on the weak interface between crystal lattices in the case of the free surface of the rock sample was under-constraint. With the continuous impact of the jet, the initial erosion pit gradually deepened and expanded under the action of the water-hammer pressure, and circumferential and radial cracks began to occur at the bottom of the pit along the crystal-lattice gap. Subsequently, the high-speed fluid entered the crack and preferentially penetrated the side of the impact surface to form macroscopic cracks under water-wedge pressure. Finally, through the erosion of the jet, the surface of rock specimen was stripped in flakes, forming an irregular pit.

The experimental results indicated that the SSPWJ produced large-scale volume damage on the granite surface through erosion, and the average volume of the erosion pit was 4.68 cm^3. The SSPWJ can reach the threshold pressure required for rock-breaking without high-pressure components and additional power components. It is not only inexpensive but also practical. The research results lay a foundation for promoting the field application of pulsed jets.

6 Conclusions

(1) A generation method for SSPWJ is proposed. Through the structural design of the device and the connection of the pipeline, an SSPWJ with an adjustable pulse pressure, pulse frequency, and pulse duration can be formed by the mutual feedback of the travel distance of the valve core and piston under the continuous injection of hydraulic oil and low-pressure water.

(2) The regularity of the jet pressure and the shape of the jet were examined. The rise, stability, and decline of the jet pressure corresponded to the three stages of piston stroke acceleration, uniform speed, and deceleration, respectively. The measured pressure ratio was consistent with the theoretical design value, confirming the feasibility of the proposed method.

(3) As the inlet flow rate in the stroke stage of the piston increased, the pulse pressure and pulse frequency increased, and the pulse duration decreased. As the inlet flow rate in the backward-stroke stage of the piston increased, the pulse frequency increased, and the pulse pressure and pulse duration remained unchanged. The effects of the structural parameters of the device on the pulse frequency and pulse duration need to be studied further.

(4) The SSPWJ can reach the threshold pressure required for rock-breaking. Flake spalling was caused mainly by shear failure and tensile failure on the granite surface under the combined action of the water-hammer pressure, high-speed lateral flow, and high-frequency dynamic load. The proposed method lays a foundation for promoting the field application of pulsed jets.

Acknowledgements
Not applicable.

Author Contributions
YL, LW and QY was in charge of the whole trial; YL wrote the manuscript; ZG and JT assisted with sampling and laboratory analyses; YYL and YZ assisted with structural design. All authors read and approved the final manuscript.

Authors' Information
Zhaolong Ge, born in 1982, is currently a professor at *State Key Laboratory of Coal Mine Disaster Dynamics and Control,* and *National & Local Joint Engineering Laboratory of Gas Drainage in Complex Coal Seam, Chongqing University, China*. His research interests include high-pressure water jet, hydraulic fracturing and coalbed methane extraction.
Yuanfei Ling, born in 1990, is currently a PhD candidate at *State Key Laboratory of Coal Mine Disaster Dynamics and Control,* and *National & Local Joint Engineering Laboratory of Gas Drainage in Complex Coal Seam, Chongqing University, China*. His research interest is high-pressure water jet.
Jiren Tang, born in 1984, is currently an associate professor at *State Key Laboratory of Coal Mine Disaster Dynamics and Control,* and *National & Local Joint Engineering Laboratory of Gas Drainage in Complex Coal Seam, Chongqing University, China*. His research interests include high-pressure water jet and supercritical carbon dioxide fracturing.
Yiyu Lu, born in 1971, is currently a professor at *College of Source and Safety, Chongqing University, China*. His research interests include high-pressure water jet, hydraulic fracturing and control of mine disaster.
Yangkai Zhang, born in 1994, is currently a PhD candidate at *State Key Laboratory of Coal Mine Disaster Dynamics and Control,* and *National & Local Joint Engineering Laboratory of Gas Drainage in Complex Coal Seam, Chongqing University, China*. His research interest is high-pressure water jet.
Lei Wang, born in 1995, is currently a master candidate at *State Key Laboratory of Coal Mine Disaster Dynamics and Control,* and *National & Local Joint Engineering Laboratory of Gas Drainage in Complex Coal Seam, Chongqing University, China*. His research interest is high-pressure water jet.
Qi Yao, born in 1996, is currently a master candidate at *State Key Laboratory of Coal Mine Disaster Dynamics and Control,* and *National & Local Joint Engineering Laboratory of Gas Drainage in Complex Coal Seam, Chongqing University, China*. His research interest is high-pressure water jet.

Funding
Supported by National Natural Science Foundation of China (Grant Nos. 51774055, 51625401), National Natural Science Foundation of Chongqing (Grant No. cstc2018jcyjAX0542), and Changjiang Scholar Program of Chinese Ministry of Education (Grant No. IRT17R112).

Competing Interests
The authors declare no competing financial interests.

Author Details
[1]State Key Laboratory of Coal Mine Disaster Dynamics and Control, Chongqing University, Chongqing 400030, China. [2]National & Local Joint Engineering Laboratory of Gas Drainage in Complex Coal Seam, Chongqing University, Chongqing 400030, China. [3]College of Source and Safety, Chongqing University, Chongqing 400030, China.

Received: 7 April 2020 Revised: 8 April 2021 Accepted: 29 March 2022
Published online: 04 May 2022

References

[1] A W Momber. Fluid jet erosion as a non-linear fracture process: A discussion. *Wear*, 2001, 250(1-12): 100–106.
[2] A W Momber. An SEM-study of high-speed hydrodynamic erosion of cementitious composites. *Wear*, 2003, 34(2): 135-142.
[3] S Y Liu, Y M Cui, Y Q Chen, et al. Numerical research on rock breaking by abrasive water jet-pick under confining pressure. *International Journal of Rock and Ming Sciences*, 2019, 120: 41-49.
[4] Y Y Lu, F Huang, X C Liu, et al. On the failure pattern of sandstone impacted by high-velocity water jet. *International Journal of Impact Engineering*, 2015, 76: 67-74.
[5] G S Li, Z H Shen, C S Zhou, et al. Investigation and application of self-resonating cavitating water jet in petroleum engineering. *Petroleum Science and Technology*, 2005, 23(1): 1-15.
[6] M M Vijay, J Remisz, X Shen. Potential of pulsed water jets for cutting and fracturing of hard rock formations. *International Journal of Surface Mining and Reclamation*, 1993, 7(3): 121-132.
[7] J E Field. Liquid impact: Theory, experiment, applications. *Wear*, 1999, 233–235: 1–12.
[8] C F Kennedy, J E Field. Damage threshold velocities for liquid impact. *Journal of Materials Science*, 2000, 35: 5331-5339.
[9] A W Momber. The response of geo-materials to high-speed liquid drop impact. *International Journal of Impact Engineering*, 2016, 89: 83-101.
[10] Z A Wang, Y Kang, X C Wang, et al. Effects of modulation position on the impact performance of mechanically modulated pulsed water jet. *Journal of Manufacturing Processes*, 2020, 56: 510-521.
[11] Y Liu, J P Wei, T Ren, et al. Experiment study of flow field structure of interrupted pulsed water jet and breakage of hard rock. *International Journal of Rock Mechanics and Mining Sciences*, 2015, 78: 253-261.
[12] A Polyakov, A Zhabin, E Averin, et al. Generated equation for calculating rock cutting efficiency by pulsed water jets. *Journal of Rock Mechanics and Geotechnical Engineering*, 2019, 11: 867-873.
[13] H S Li, S Y Liu, J G Jia, et al. Numerical simulation of rock-breaking under the impact of self-excited oscillating water jet. *Tunnelling and Underground Space and Technology*, 2020, 96: 103179.
[14] S Dehkhoda, N K Bourne. Production of a high-velocity water slug using an impact technique. *Review of Scientific instruments*, 2014, 85(2): 1-5.
[15] G Rehbinder. Investigation of water jet pulses generated by an impact piston device. *Applied Scientific Research*, 1983, 40(1): 7-37.
[16] S Dehkhoda, M Hood, H Alehossein, et al. Analytical and experimental study of pressure dynamics in a pulsed water jet device. *Flow, Turbulence and Combustion*, 2012, 89: 97-119.
[17] Y Liu, J P Wei. On the formation mechanism and characteristics of high-pressure percussion pulsed water jets. *Fdmp-fluid Dynamics & Materials Processing*, 2015, 11(3): 221-240.
[18] S Dehkhoda, M Hood. An experimental study of surface and sub-surface damage in pulsed water-jet breakage of rocks. *International Journal of Rock Mechanics & Mining Sciences*, 2013, 63: 138-147.
[19] S Dehkhoda, M Hood. The internal failure of rock samples subjected to pulsed water jet impacts. *International Journal of Rock Mechanics & Mining Sciences*, 2014, 66: 91-96.
[20] P Raj, S Hloch, R Tripathi, et al. Investigation of sandstone erosion by continuous and pulsed water jets. *Journal of Manufacturing Processes*, 2019, 42: 121-130.
[21] M Zelenak, J Foldyna, J Scucka, et al. Visualisation and measurement of high-speed pulsating and continuous water jets. *Measurement*, 2015, 72: 1-8.
[22] S Hloch, A Nag, F Pude, et al. On-line measurement and monitoring of pulsating saline and water jet disintegration of bone cement with frequency 20 kHz. *Measurement*, 2019, 147: 106828.
[23] D Hu, X H Li, C L Tang, et al. Analytical and experimental investigations of the pulsed air-water jet. *Journal of Fluids and Structures*, 2015, 54: 88-102.
[24] Y P Qu, S Y Chen. Orthogonal experimental research on the structure parameters of a self-excited pulsed cavitation nozzle. *European Journal of Mechanics B/Fluids*, 2017, 65: 179-183.
[25] D Li, Y Kang, X L Ding, et al. Effects of area discontinuity at nozzle inlet on the characteristics of high speed self-excited oscillation pulsed waterjets. *Experimental Thermal and Fluid Science*, 2016, 79: 254-265.
[26] D Li, Y Kang, X L Ding, et al. Effects of area discontinuity at nozzle inlet on the characteristics of self-resonating cavitating waterjet. *Chinese Journal of Mechanical Engineering*, 2016, 29(3): 813-824.
[27] M Huang, Y Kang, X C Wang, et al. Experimental investigation on the impingement characteristics of a self-excited oscillation pulsed supercritical carbon dioxide jet. *Experimental Thermal and Fluid Science*, 2018, 94: 304-315.
[28] Y Liu, J P Wei, T Ren. Analysis of the stress wave effect during rock breakage by pulsating jets. *Rock Mechanics and Rock Engineering*, 2016, 49(2): 503-514.
[29] Y Z Xue, H Si, Q T Hu. The propagation of stress waves in rock impacted by a pulsed water jet. *Powder Technology*, 2017, 320: 179-190.
[30] H X Jiang, Z H Liu, K Gao. Numerical simulation on rock fragmentation by discontinuous water-jet using coupled SPH/FEA method. *Powder Technology*, 2017, 312: 248-259.
[31] S H Hong, K W Kim. A new type groove for hydraulic spool valve. *Tribology International*, 2016, 103: 629-640.